Biology Contribution

Preclinical Model of Stereotactic Ablative Lung Irradiation Using Arc Delivery in the Mouse: Effect of Beam Size Changes and Dose Effect at Constant Collimation

Annaïg Bertho, PhD,[*] Morgane Dos Santos, PhD,[†] Valérie Buard, BS,[*] Vincent Paget, PhD,[*] Olivier Guipaud, PhD,[*] Georges Tarlet, BS,[*] Fabien Milliat, PhD,[*] and Agnès François, PhD[*]

Institut de Radioprotection et de Sûreté Nucléaire, Service de Recherche en Radiobiologie et en Médecine régénérative, Laboratoire de Radiobiologie des expositions Médicales, Fontenay-aux-Roses, France; and †Institut de Radioprotection et de Sûreté Nucléaire, Service de Recherche en Radiobiologie et en Médecine régénérative, Laboratoire de Radiobiologie des expositions Accidentelles, Fontenay-aux-Roses, France

Purpose: Stereotactic body radiation therapy is a therapeutic option offered to high surgical risk patients with lung cancer. Focal lung irradiation in mice is a new preclinical model to help understand the development of lung damage in this context. Here we developed a mouse model of lung stereotactic therapy using arc delivery and monitored the development of lung damage while varying the beam size and dose delivered.

Methods and Materials: C57BL/6JRj mice were exposed to 90 Gy focal irradiation on the left lung using 1-mm diameter, 3×3 mm^2, 7×7 mm^2, or 10×10 mm^2 beam collimation for beam size effect and using 3×3 mm^2 beam collimation delivering 20 to 120 Gy for dose effect. Long-term lung damage was monitored with micro−computed tomography imaging with anatomopathologic and gene expression measurements in the injured patch and the ipsilateral and contralateral lungs.

Results: Both 1-mm diameter and 3×3 mm^2 beam collimation allow long-term studies, but only 3-mm beam collimation generates lung fibrosis when delivering 90 Gy. Dose-effect studies with constant 3-mm beam collimation revealed a dose of 60 Gy as the minimum to obtain lung fibrosis 6 months postexposure. Lung fibrosis development was associated with club cell depletion and increased type II pneumocyte numbers. Lung injury developed with ipsilateral and contralateral consequences such as parenchymal thickening and gene expression modifications.

Conclusions: Arc therapy allows long-term studies and dose escalation without lethality. In our dose-delivery conditions, dose-effect studies revealed that 3×3 mm^2 beam collimation to a minimum single dose of 60 Gy enables preclinical models

Introduction

The lung is a good candidate for stereotactic body radiation therapy (SBRT) because of its organization in parallel, which enables ablative dose delivery on small volumes.[1] However, SBRT for bronchopulmonary tumors may generate lung toxicity such as radiation pneumonitis or radiation-induced lung fibrosis.[2] Changing fractionation protocols is not trivial, and history has forced radiation oncologists to face up to dramatic late normal tissue damage when using hypofractionation, even moderate hypofractionation, especially with schemes including large volumes or critical organs.[3-6] Incrementing fraction size exposes late-responding tissues, characterized by a low α/β ratio, to increased damage.[1,7] This may expose patients to unexpected late aftereffects. During the past 2 decades, the ballistic accuracy of novel radiation therapy machines has allowed the return of extreme hypofractionation schemes in a safer context. However, despite the sharp reduction in the volume of exposed healthy tissues, side effects persist.[8-10]

Until now, a technological block has prevented preclinical modeling of SBRT in small animals. This was overcome about 10 years ago, thus allowing the use of high single or even fractionated doses of radiation exposure in very small volumes of mouse lung. Published data in this context demonstrated dose and volume dependency of radiation-induced lung fibrosis.[9,11] The most published model involves the use of 3-mm collimation administering a single dose of 90 Gy, thus generating radiation fibrosis in 4 weeks,[12-16] but beam collimations from 1 to 5 mm (square or circular fields) and single doses from 10 to 100 Gy have been reported.[11,16] Although the development of such models is too recent to offer an idea of a possible specificity in the lung tissue response to small-volume exposure, several studies have highlighted the importance of reduced exposed lung volumes compared with large-volume models. For example, Hong et al[16] demonstrated the lack of difference between fibrosis-prone (C57) and -resistant mice (C3H) in SBRT preclinical models as opposed to large-volume models,[17,18] suggesting different pathophysiological processes in the development of radiation-induced lung fibrosis. Volume dependency in the patterns of serum cytokine changes was also demonstrated after 90-Gy, single-dose exposure using 2- or 3.5-mm beam collimations.[15] Finally, comparing 20-Gy wide field (7-mm beam collimation) and 90-Gy small field (3-mm beam collimation), Jin et al[19] identified candidate genes and proteins specifically associated with lung radiation exposure in the SBRT configuration, reinforcing the need to build accurate models to understand the specificity of SBRT.

The use of arc delivery has been shown to avoid severe skin damage associated with single-beam high-dose delivery and to prolong study duration.[20] Our objective in the present study was to use arc therapy dose delivery to focally irradiate the mouse left lung while varying beam collimation size and to realize a dose-response study at constant collimation. The final purpose was to obtain lung fibrosis in a length of time compatible with mouse life span. We show that exposure to 90 Gy using 3×3 mm^2 beam collimation allowed the development of an injury patch evolving through tissue scarring and consolidation until 12 months postexposure without lethality. Dose-response study revealed that with this size of field and in our conditions, a dose of 60 Gy must be prescribed to guarantee lung tissue fibrosis within 6 months. Lung tissue reaction was associated with club cell depletion and increased type II pneumocyte numbers, as well as ipsilateral and contralateral repercussions such as parenchymal thickening and gene expression modifications.

Methods and Materials

Animals and irradiation procedure

Male C57BL/6JRj mice from Janvier Labs (Le Genest-Saint-Isle, France) were used for all experiments. Animals were 10 to 12 weeks old at the beginning of the experiments. Animals were housed in the IRSN animal facilities accredited by the French Ministry or Agriculture for performing experiments on rodents. Animal experiments were performed in compliance with French and European regulations on the protection of animals used for scientific purposes (EC Directive 2010/63/EU and French Decree 2013-118). All experiments were approved by the Ethics Committee 81 and authorized by the French Ministry of Research under the reference APAFIS 13021-2018011217442982 v1 (internal project number P17-13).

Focal irradiation was performed on the Small Animal Radiation Research Platform (Xstrahl) using arc therapy as already described.[20] For irradiation, mice were anesthetized with 100 mg/kg ketamine (Imalgene 1000, Merial, Lyon, France) and 10 mg/kg xylazine (Rompun 2%, Bayer Healthcare, Loos, France) to create profound anesthesia and limit as far as possible respiratory motion. Anesthetized mice were immobilized on the treatment bed, and the isocenter was placed on the left lung on the cone beam computed tomography (CT) image using the treatment planning system Muriplan. Cone beam CT images were obtained using an

uncollimated beam (20 × 20 cm), a voltage of 60 kV, and an intensity of 0.8 mA, with an inherent and additional filtration of 0.8 and 1 mm of beryllium and aluminum, respectively, with continuous beam on and 360° (horizontal) stage rotation between the x-ray source and the digital flat panel detector. A total of 236 projections were obtained, and a 3-dimensional reconstruction image of the mouse was transferred to the dose-planning, verification, and delivery Muriplan system. The treatment planning system was calibrated by Xstrahl. After image segmentation into air, lung, fat, tissue, and bone, we then placed the isocenter within the left lung. Irradiations were performed at 220 kV and 13 mA with inherent and additional filtrations of about 0.8 and 0.15 mm of beryllium and copper, respectively. The half value layer is about 0.667 mm of copper, and the resulting energy spectrum has an effective energy of 69 keV. For collimation-effect studies, the left lung was exposed to a 90-Gy single dose using 4 different collimators: 1-mm diameter, 3×3 mm^2, 7×7 mm^2, and 10×10 mm^2. For reasons of convenience, these collimators will be called 1, 3, 7 and 10 mm, respectively. The 7-mm collimator was not provided by Xstrahl in our standard configuration of the Small Animal Radiation Research Platform; to irradiate the entire left lung, but avoid the right lung as much as possible, we designed a homemade 7×7 mm^2 collimator. This collimator and validation of the experimental dosimetry are described in Methods and Materials E1.

For collimation effect, lung tissue was harvested 1, 3, 6, and 12 months after radiation exposure. For dose-effect studies, mice were irradiated using 3-mm collimation at single doses of 20, 40, 60, 80, 100, and 120 Gy. Lung tissue was harvested at 1 and 6 months postexposure. To avoid variations in the structural/cellular constitution of different areas of the lung, control/unirradiated mice were included for lung imaging and histologic analyses, and measurements were performed in matched areas between irradiated and nonirradiated mice.

Micro-CT imaging

Mice were anesthetized by inhalation of 1.5% isoflurane. Mouse lung imaging was performed using a micro-CT scanner (Quantum FX, PerkinElmer) with respiratory gating. The images were acquired at 90 kV, 160 μA, with no additional filtration and with a field of view of about $20 \times 20 \times 20$ mm for a resolution of 40 μm. The estimated shooting time was about 4 minutes and 30 seconds, and 512 slices were acquired. The mean dose absorbed by the mice was about 1653 mGy. Images were analyzed with AnalyzePro software, which allows semiautomatic and manual segmentation. The main bronchi and right and left lungs were segmented using the semiautomatic option with the same threshold range to enable comparison. Lesions induced by irradiation, the injury patch, were manually contoured by the same operator. From these segmentations, volumes were computed; for each volume, Hounsfield unit (HU) histograms were extracted using a bin width of 1 HU. For density distribution representation, smoothing curves were constructed using PRISM software applying second-order smoothing with 60 neighbors.

Lung tissue treatment

For histology, right and left lungs were removed, fixed in 4% paraformaldehyde, and embedded in paraffin. Five-micrometer paraffin tissue sections were used for hematoxylin-eosin-saffron (HES) and Masson trichrome staining and for immunohistological studies. For mRNA preparation, lung tissues (injury patch, ipsilateral lung, and contralateral lung) were frozen in RNAlater RNA Stabilization Reagent (Qiagen, Valencia, CA) until analysis. The left lung was cut to separate the patch area from the ipsilateral lung, always using the same scheme, thus standardizing tissue harvesting for conditions in which the patch was not visible.

HES- and Masson trichrome–stained tissue sections were used to assess lesion severity. Measurements of the thickness of the alveolar septa, bronchiole diameter, and cell counts were performed using the VisioL@b 2000 image analysis software (Biocom SA, Les Ulis, France). Thickness of the alveolar septa was measured in 5 different fields (×400 magnification) with 20 measurements per field performed close to the patch (septa were destroyed within the injured area) or in the pleural area (ie, far from the patch near the lung pleura).

Immunostaining

Sections were incubated with antibodies to prosurfactant protein C, uteroglobin, or von Willebrand factor, all in coimmunostaining with alpha-smooth muscle actin to facilitate structure visualization and to look for possible epithelial- or endothelial-to-mesenchymal transition. All antibodies were from Abcam, Paris, France. Samples were then incubated with corresponding Alexa fluor-conjugated secondary antibodies (Life Technologies, Saint-Aubin, France). Sections were mounted in VECTASHIELD mounting medium with DAPI (Eurobio AbCys, Courtaboeuf, France). Uteroglobin-positive cells were counted in 3 different bronchioles per sample in the injured area and expressed as a percentage of the total cells counted along the epithelial axis. Prosurfactant protein C-positive cells were counted in 10 successive fields (objective 40) near the injury patch and close to the pleural area (far from the patch).

Tissue RNA extraction and quantitative real-time polymerase chain reaction

Total RNA was prepared with the mirVana isolation kit (Thermo Fisher Scientific, France). After quantification on a NanoDrop ND-1000 apparatus (NanoDrop Technologies, Rockland, DE), reverse transcription was performed with 1 μg of RNA using a reverse transcription kit from Applied Biosystems (Courtaboeuf, France). Relative mRNA was
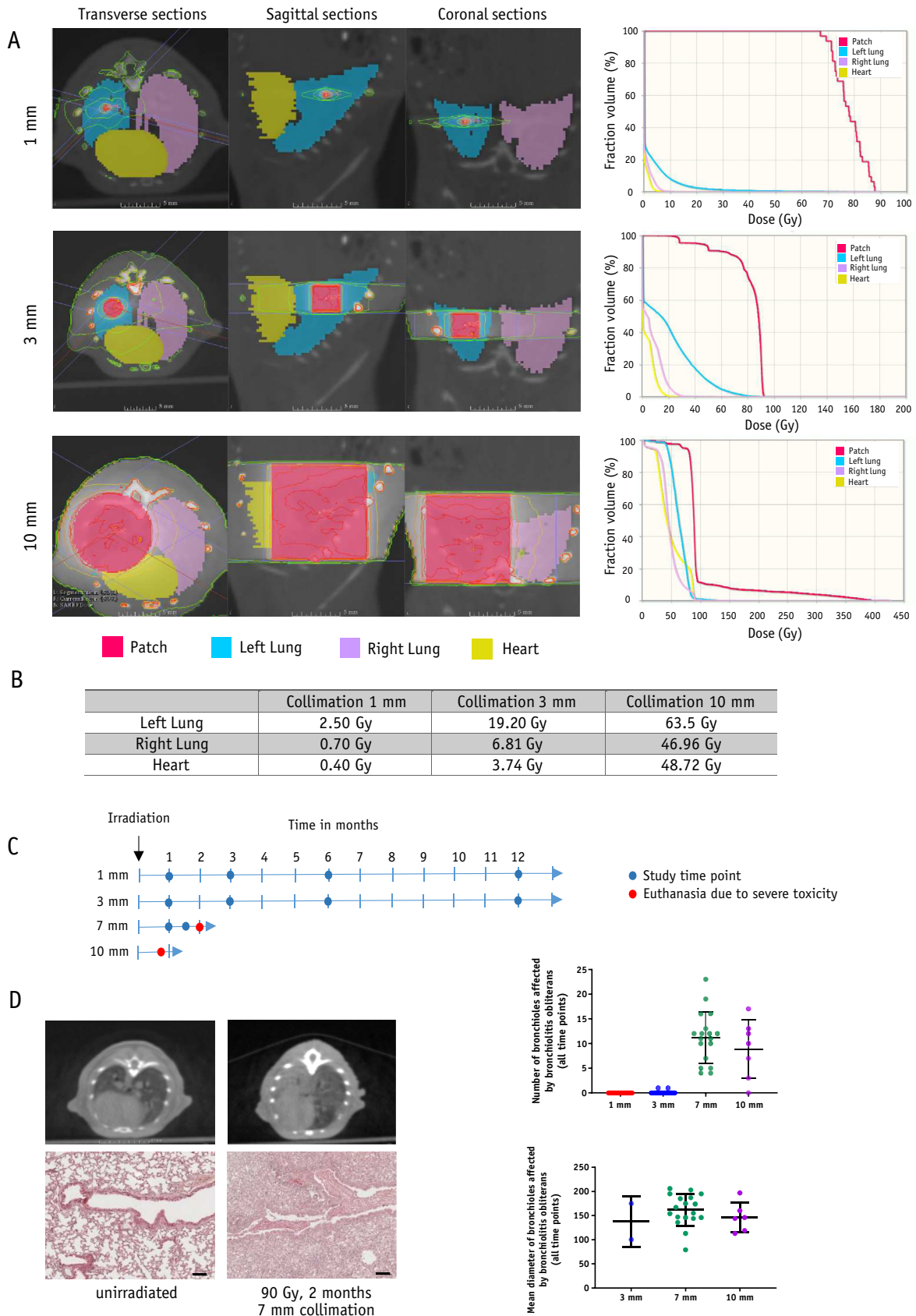
Fig. 1. Left lung arc therapy: effect of variations in beam size. (A) Isodose curves, organ contouring, and dose-volume histograms using 1-mm, 3-mm, or 10-mm beam collimation. (B) Examples of mean doses received by the left lung, the right lung, and the heart using different collimation sizes. (C) Experimental schedules. 4 < n < 8 per group. (D) Example of

quantified using the $\Delta\Delta CT$ method with 18S as house-keeping gene. Genes were chosen as lung cell markers or according to their proven role in lung tissue inflammatory response to radiation exposure. mRNA levels were not measured after irradiation with 10-mm collimation given the severity of radiation damage and the short duration of the experimental period owing to anticipated euthanasia. For 1- and 3-mm collimation, mRNA was measured in the injured patch, in the ipsilateral lung, and in the contralateral lung. For 7-mm collimation, the injury patch included all the left lung, and so mRNA was measured in the left lung and right lung.

Genes measured are listed in Table E1.

Statistical analyses

Data are given as means ± standard error of the mean. Statistical analyses were performed by analysis of variance (Tukey multiple comparison posthoc test) or Student's t test, with a level of significance of $P < .05$.

Results

Effect of variations in beam size

Bronchiolitis obliterans limits mouse survival at large beam size

As shown in Figure 1A, increasing the size of beam collimation moved the dose-volume histogram of each contoured organ closer to that of the target area. Examples of mean doses are given in Figure 1B. Animals exposed to 90 Gy with 7- or 10-mm collimation required euthanasia at 2 months and 21 days, respectively, because of severe toxicity (Fig. 1C). Large-volume irradiation was associated with bronchiolitis obliterans (Fig. 1D, left panel). Figure 1D (right panel) shows the number of bronchioles affected by bronchiolitis obliterans and their diameter. Bronchiolitis obliterans was never observed at 1 mm, was rare at 3 mm, and concerned almost all bronchioles at 7- and 10-mm collimation.

Exposure using 3-mm beam collimation generates long-term tissue fibrosis

Tissue damage was characterized by total parenchymal disruption concerning more than 50% of the total tissue section for 7-mm collimation and the entire section for 10-mm collimation (Fig. 2A). Both configurations were associated with increased thickness of the alveolar septa of the entire left lung (Fig. 2B).

The use of 1-mm collimation generated an injury patch visible on tissue sections at 1 and 3 months (Fig. 2A), accompanied by thickened alveolar septa, including in the right lung at 1 month (Fig. 2B, Fig. E1A). The alveolar septa remained thickened until 12 months postexposure. The injury patch was never visible on CT scans (Fig. 2C) and did not change the position of the mean smoothed HU curve (Fig. 2D).

Irradiation with 3-mm collimation generated an injury patch at 1 month that lasted until 12 months. Alveolar septa were severely thickened up to 12 months (Fig. 2B, Fig. E1A for right lung). Stricture occurred with tissue scarring because the patch volume decreased with time (Fig. E1B). Mean smoothed HU curves show increased intensity of the patch from 1 to 12 months, with curve shift signaling increased density of the left lung at 1 month (Fig .2D).

Beam size affects type II pneumocyte and bronchiolar epithelial cell numbers

Figure 3A (left panel) shows representative pictures of UGB immunostaining. Graphics show UGB-positive cell counts revealing significant club cell depletion in the injured area, with repercussion in the right lung for 7- and 10-mm beam collimation. Irradiation with 1-mm collimation had no effect on UGB-positive cell numbers.

Figure 3B (left panel) shows representative pictures of SFTPC/αsma immunostaining. Radiation exposure induced an increase in the number of type II pneumocytes with 1- and 3-mm beam collimation in the injury patch and close to the patch, respectively. Higher irradiated volumes did not generate increased type II pneumocyte numbers, except for the 1.5-month time point after 7-mm beam collimation in the pleural area.

Acute modifications of inflammatory gene expression levels extend to the contralateral lung despite the collimation used

Given the damage generated after 10-mm beam collimation, we decided to exclude these samples from gene measurements. To simplify graph reading, control values were checked for similarity throughout the experimental period and pooled to obtain only 1 value per tissue (Fig. 4).

Overall (Fig. 4A), 90-Gy irradiation using 7-mm collimation was associated with severe CCSP gene expression downregulation and no SFTPC gene expression upregulation. Reducing the irradiated collimation to 3 mm preserved CCSP gene expression and induced SFTPC gene expression upregulation in the patch and the ipsilateral and right lungs. Using 1-mm collimation upregulated CCSP in the injury patch and the right lung at 12 months and induced strong acute responsive SFTPC upregulation. Modifications

---

scanner images and HES-stained tissue sections showing bronchiolitis obliterans compared with unirradiated tissue 2 months after 90 Gy exposure using 7-mm beam collimation. Bar: 100 μm. Graphics show the number (upper panel) and the mean diameter (in μm, lower panel) of bronchioles affected by bronchiolitis obliterans, regardless of time point. Each point represents the value for 1 animal (1 tissue section). Diameter values represent the mean of diameters measured for all bronchioles affected by bronchiolitis obliterans in 1 tissue section.
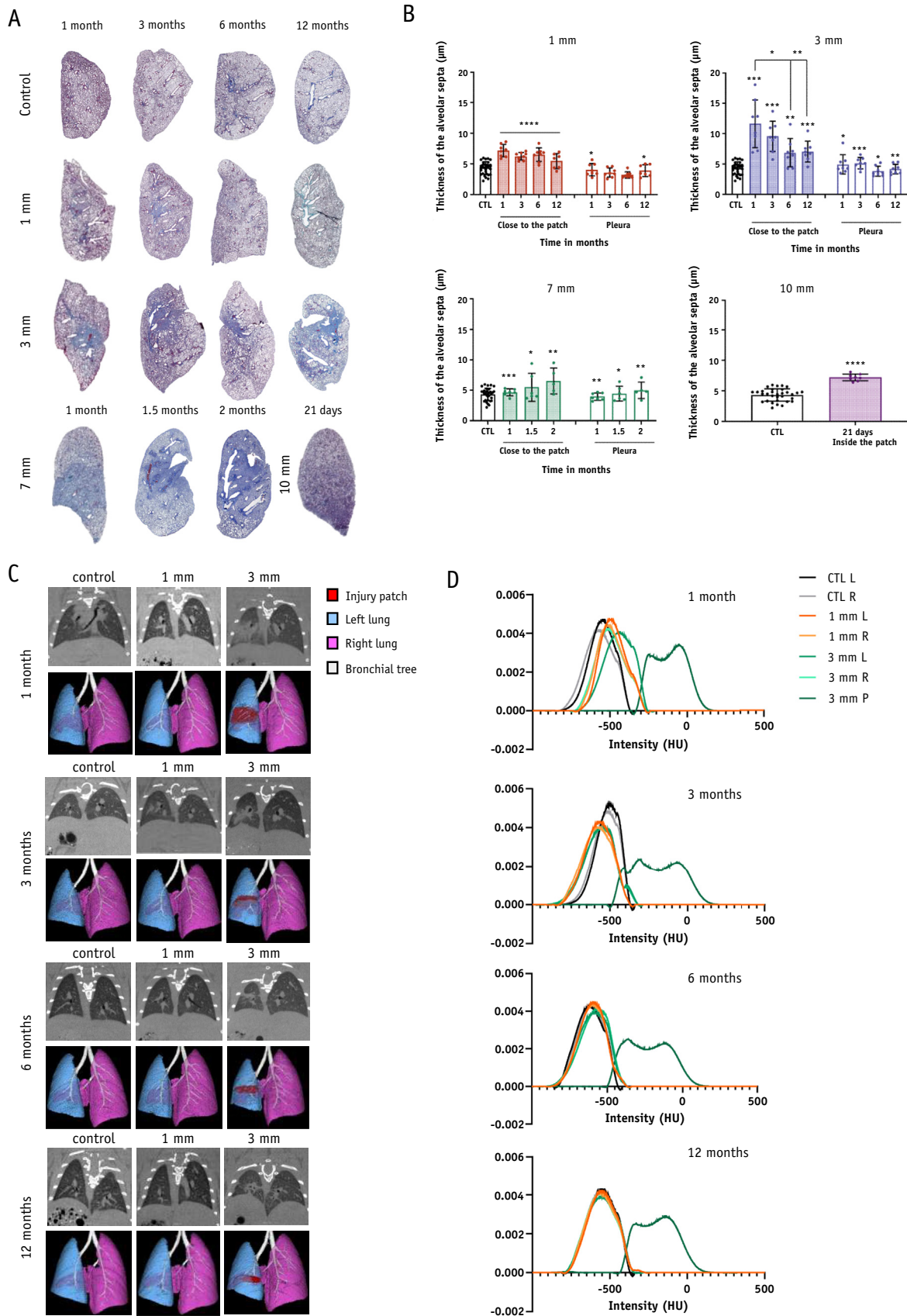
Fig. 2. Varying beam size: histology and imaging. (A) Representative left lung histologic sections after Masson trichrome staining from 1 to 12 months postexposure for 1- and 3-mm collimation; at 1, 1.5, and 2 months postexposure for 7-mm

in the expression of Cyp2F2 (for club cells) and Foxj1 (for ciliated cells) showed the same profiles (Fig. E2).

The 7-mm collimation induced strong upregulation of IL-1β, IL-6, TNF, CXCL2, and EMR1, with downregulation of ENG (Fig. 4B, Fig. E3). The same profiles were obtained in the right lung. Using 1- or 3-mm collimation generated similar profiles of acute (1-month) inflammatory gene expression levels in the injury patch and the ipsilateral and right lungs, except for CXCL2 upregulation, which was observed only with 3-mm collimation.

Dose effect

Tissue fibrosis occurs after exposure to 60 Gy or more

Localized lung opacification was observable from 80 Gy at 1 month and from 60 Gy at 6 months (Fig. 5A). Smoothed mean intensity representation (in HU) highlights the presence of a dense injury patch at 1 month after 80-, 100-, and 120-Gy doses (Fig. 5B, left panel). The 40- and 60-Gy doses generated a slight shift of the corresponding curves, whereas the 20 Gy curve remained similar to controls. At 6 months (Fig. 5B, right panel), the 60-Gy curve clearly joined the "condensed" group of higher doses (80, 100, and 120 Gy). Injury patch volume, represented as a percentage of total lung volume in Figure 5C, reflected well the appearance of a visible injury patch 6 months after 60 Gy.

Histologic sections confirmed the presence of an injury patch (Fig. 5D, arrowheads) 1 month after 80, 100, and 120 Gy. Doses of 40 and 60 Gy generated noticeable damage, albeit undetectable with CT scans. At 6 months, a patch clearly appeared after 60 Gy, similar in size and density to patches at other high doses.

Thickness of the alveolar septa was measured as a proxy of lung parenchymal response to trauma (Fig. 5E). Tissue response from 40 Gy occurred at 1 month, with acute repercussions for the patch in the pleural area and right lung at doses of 80, 100, and 120 Gy. At 6 months, the septa returned to control values at 40 Gy and remained significantly thickened at 60 to 120 Gy, with repercussions on the right lung.

Dose effect on club cells and type II pneumocytes

Figure 6A shows significant club cell depletion for doses of 40 Gy and above. The number of cells per 100 μm of bronchiolar epithelium did not change significantly (Fig. 6B). At 6 months, depletion was noted for all doses from 20 to 120 Gy (Fig. 6A). Repercussions occurred in the right lung, with significant cell loss after 100 and 120 Gy. The number of cells per 100 μm decreased significantly from 40 to 120 Gy in the left lung and after 100 and 120 Gy in the right lung (Fig. 6B).

Exposure to 60 Gy or less induced type II pneumocyte hyperplasia at 1 month, whereas higher doses induced type II pneumocyte depletion (Fig. 6C). Significant repercussions occurred in the right lung after 120 Gy. At 6 months, the increase in type II pneumocyte numbers was significant after all doses except 20 Gy. No change occurred in the right lung.

mRNA expression

Irradiation induced a dose-dependent decrease in CCSP gene expression at 1 month in the injury patch (Fig. E4A). At 6 months, CCSP expression levels were similar to control values. This was confirmed by Cyp2F2 expression profiles (Fig. E5). At 1 month, irradiation decreased SFTPC mRNA expression, especially in the ipsilateral and right lungs. At 6 months, expression returned to control values. Figure E4B shows a strong IL-6 overexpression in the injury patch. An impact on the right lung was visible only after 120 Gy. IL-6 overexpression persisted at 6 months in the patch, with effects on the right lung after 120 Gy. Figure E6 shows other gene expression modifications.

Discussion

SBRT is guided today more by technical advances than by radiobiological knowledge. In this study, we used our model of focal lung irradiation in mice using arc therapy to yield information on the development of lung damage, depending on dose or beam size in this context.

To study the effect of varying beam size, we chose a single dose of 90 Gy, a dose extensively used in the different reports published since the advent of the technical possibility of focal irradiation of the lung in mice. However, most studies were short-term because of severe damage to the skin and/or muscles, such as hair loss and

collimation; and at 21 days postexposure for 10-mm collimation. (B) Thickness of the alveolar septa (in μm) measured in controls and close to the injury patch or in the pleural area from 1 to 12 months postexposure for 1- and 3-mm collimation; at 1, 1.5, and 2 months postexposure for 7-mm collimation and at 21 days postexposure for 10-mm collimation. Control histograms regroup the values of all measurements performed from 1 to 12 months. 5 < n < 8 except for control, n = 32. (C) Representative micro−computed tomography images and 3-dimensional reconstructions from 1 to 12 months after 90 Gy exposure using 1- and 3-mm beam collimation. Different colors have been used to differentiate the injury patch (red), the left lung (blue), the right lung (pink), and the main bronchi (white). (D) Smoothed mean intensity representation in Hounsfield units (HU) in the injured area (patch when visible, left lung otherwise and right lung) from 1 to 12 months postexposure using 1-mm (orange colors) or 3-mm beam collimation (green colors) compared with controls (gray and black). 4 < n < 8 per group. *P < .05. **P < .01. ***P < .001. ****P < .0001. (A color version of this figure is available at https://doi.org/10.1016/j.ijrobp.2020.03.011.)
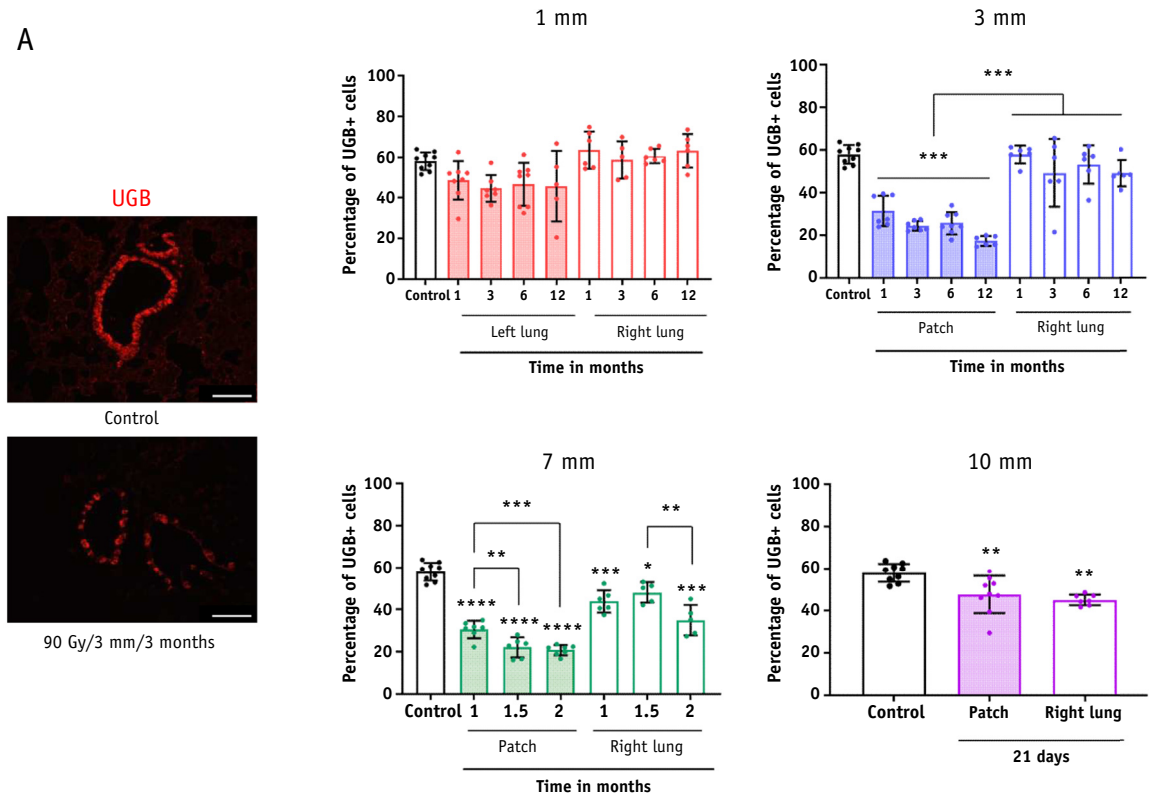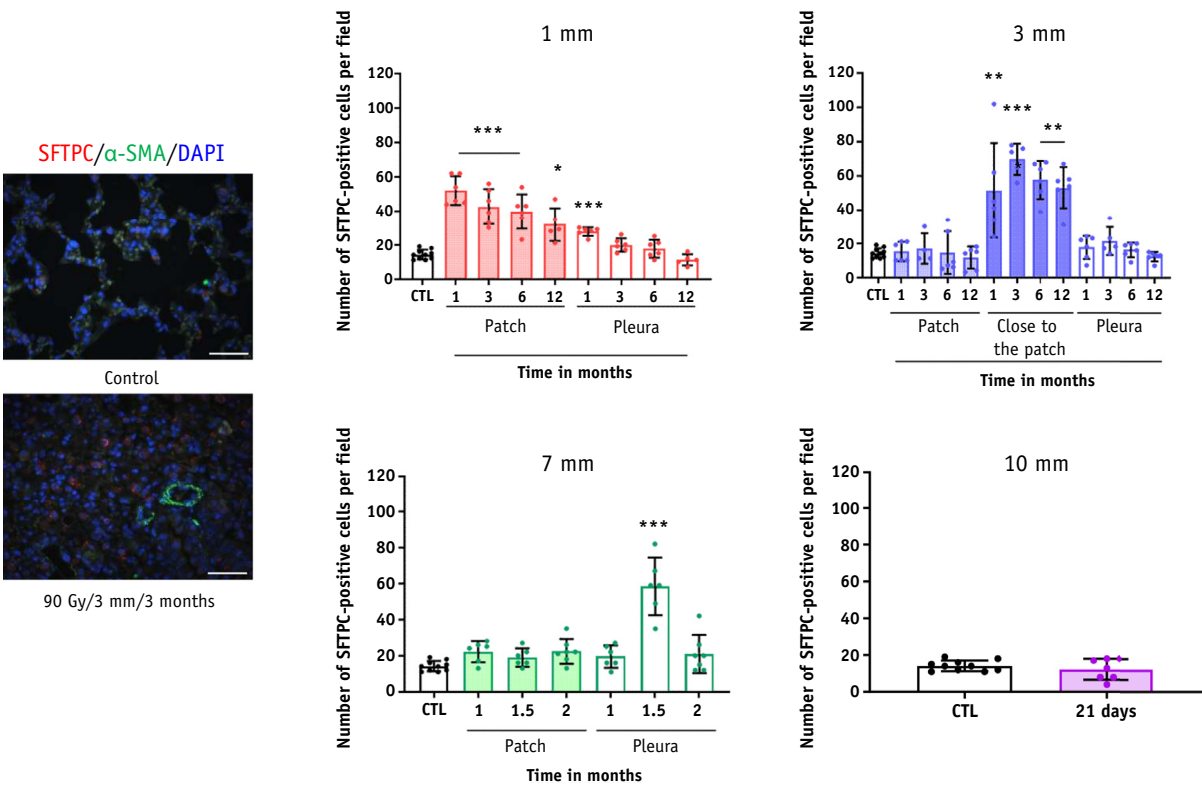
Fig. 3.   Effect of varying beam size on club cell and type II pneumocyte numbers. (A) Representative pictures of utero-globin immunostaining (club cells) in control and irradiated tissues 3 months after 90 Gy exposure using 3-mm beam

dermonecrosis, as reported by Kwon et al.[12-14,16,19] Here we show that arc therapy allowed long-term studies until 12 months postexposure, at least with 1- or 3-mm beam collimation. Arc therapy dose delivery has 3 main advantages: (1) it prevents severe damage to the skin and underlying structures; (2) it allows a more targeted definition of the irradiated volume because the single beam irradiates a core part of the body, which corresponds to a higher volume when using the same collimation; and (3) CT scan allows lung damage to be followed.

Acute lung damage was characterized by dense/hypercellular inflammation and a total disruption of alveolar organization, as already described.[20] The use of 7- or 10-mm beam collimation induced severe bronchiolitis obliterans, which was the reason for euthanasia of the animals. Airway obliteration and whole left-lung consolidation was also observed using 5-mm collimation (90 Gy) in the study by Hong et al,[16] highlighting the determinant role of beam size in the tolerance of exposure to such high doses.

Following radiation-induced lung injury using CT scan remains a challenge in the clinic.[21] In preclinical models, micro-CT imaging has been shown to be a sensitive technique for the assessment of late lung toxicity[22] but appeared insufficient to follow mitigation effects ensured by nintedanib administration.[23] The ability to follow lung damage by CT imaging remains an important noninvasive parameter to be taken into account in the choice of preclinical models of radiation-induced lung damage. In our study, acute lung damage induced with 1-mm collimation was not visible using CT imaging and did not modify HU curves despite visible damage on tissue sections, illustrating the aforementioned limits of CT imaging. No opacification occurred at later time points, confirmed by histological observations demonstrating no tissue fibrosis. Only 3-mm collimation was associated with visible opacification on CT scan and HU curve shift until 12 months postexposure.

Use of 3-mm collimation destroyed a significant number of club cells and was associated with an increase in type II pneumocyte numbers. Club cells are quiescent in homeostatic epithelium but are able to self-renew in cases of damage and generate club, goblet, and ciliated cells, or even type I and II alveolar cells, to maintain homeostasis of

bronchiolar walls.[24] Using a transgenic mouse model of conditional club cell depletion, Perl et al demonstrated compromised lung epithelial repair and peribronchiolar fibrosis.[25] Chronic club cell depletion obtained after repeated exposure to naphthalene induced fibroblast proliferation and peribronchiolar collagen deposition and was demonstrated as a good model for lung fibrosis.[26] On the other hand and unexpectedly, naphthalene-induced acute club cell depletion attenuates bleomycin-induced lung fibrosis in mice.[27] Authors hypothesize that protection may involve well-described rapid club cell recovery after a single naphthalene injection. Finally, whole-thorax radiation exposure to 15 Gy in mice is associated with club cell depletion and reduced CCSP mRNA abundance that may potentiate influenza A virus infection−induced lung epithelial damage.[28] In our study, club cells were chronically depleted, and this depletion was detected when the irradiated volume was sufficient to include a significant proportion of bronchioles, as in the case of 3-mm collimation. As observed in studies cited earlier, club cell depletion may also play a significant role in radiation-induced fibrosis in our model.

Type II pneumocytes also show stem cell properties and produce type I pneumocytes to regenerate the lung alveolar space in the case of injury.[29,30] Impaired type II pneumocyte proliferation and subsequent loss of or abnormal alveolar repair capacity have been implicated in the development of chronic obstructive pulmonary disease in humans.[31] Type II pneumocytes have been shown to play a critical role in lung fibrosis development,[32] and targeted injury of type II pneumocytes is sufficient to induce pulmonary fibrosis.[33] Österreicher et al reported an acute (within 3 weeks) dose-dependent decrease in type II pneumocyte numbers after thoracic irradiation from 1 to 25 Gy.[34] Type II pneumocyte depletion was also observed by Citrin et al after 17.5 Gy whole-thorax irradiation in mice.[35] In contrast, increased proliferation/hyperplasia of type II pneumocytes has also been observed 4 weeks and 5 months after 10 or 12 Gy thoracic irradiation in mice.[36] We previously showed that 17 Gy whole-thorax irradiation increased the number of type II pneumocytes,[37] suggesting alveolar reconstruction as reported by Almeida et al 5 months after both single and fractionated whole thorax

collimation. Bar: 100 μm. Graphics show the percentages of UGB-positive cells in the bronchiolar epithelium in control lungs and in the injury patch and right lungs at different time points after 90 Gy exposure using 1-, 3-, 7-, or 10-mm beam collimation. Significance symbols without a line mean that groups are compared with unirradiated control. 6 < n < 8. Control value represents the pooled data of 1- and 12-month control tissues (n = 9). (B) Representative pictures of prosurfactant protein C (red) and alpha smooth muscle actin (green) immunostaining in control and irradiated tissues 3 months after 90 Gy exposure using 3-mm beam collimation. Bar: 100 μm. Graphics show the percentages of SFTPC-positive cells per field in the parenchyma of control lungs and in the injury patch and pleural side of the left lungs at different time points after 90 Gy exposure using 1-, 3-, 7-, or 10-mm beam collimation. For the 3-mm beam collimation, a supplemental measurement was performed close to the patch due large SFTPC-positive cell numbers around the damaged area in this configuration. Significance symbols without a line mean that groups are compared with unirradiated control. Control value represents the pooled data of 1- and 12-months control tissues (n = 10). *$P < .05$. **$P < .01$. ***$P < .001$. ****$P < .0001$. (A color version of this figure is available at https://doi.org/10.1016/j.ijrobp.2020.03.011.)
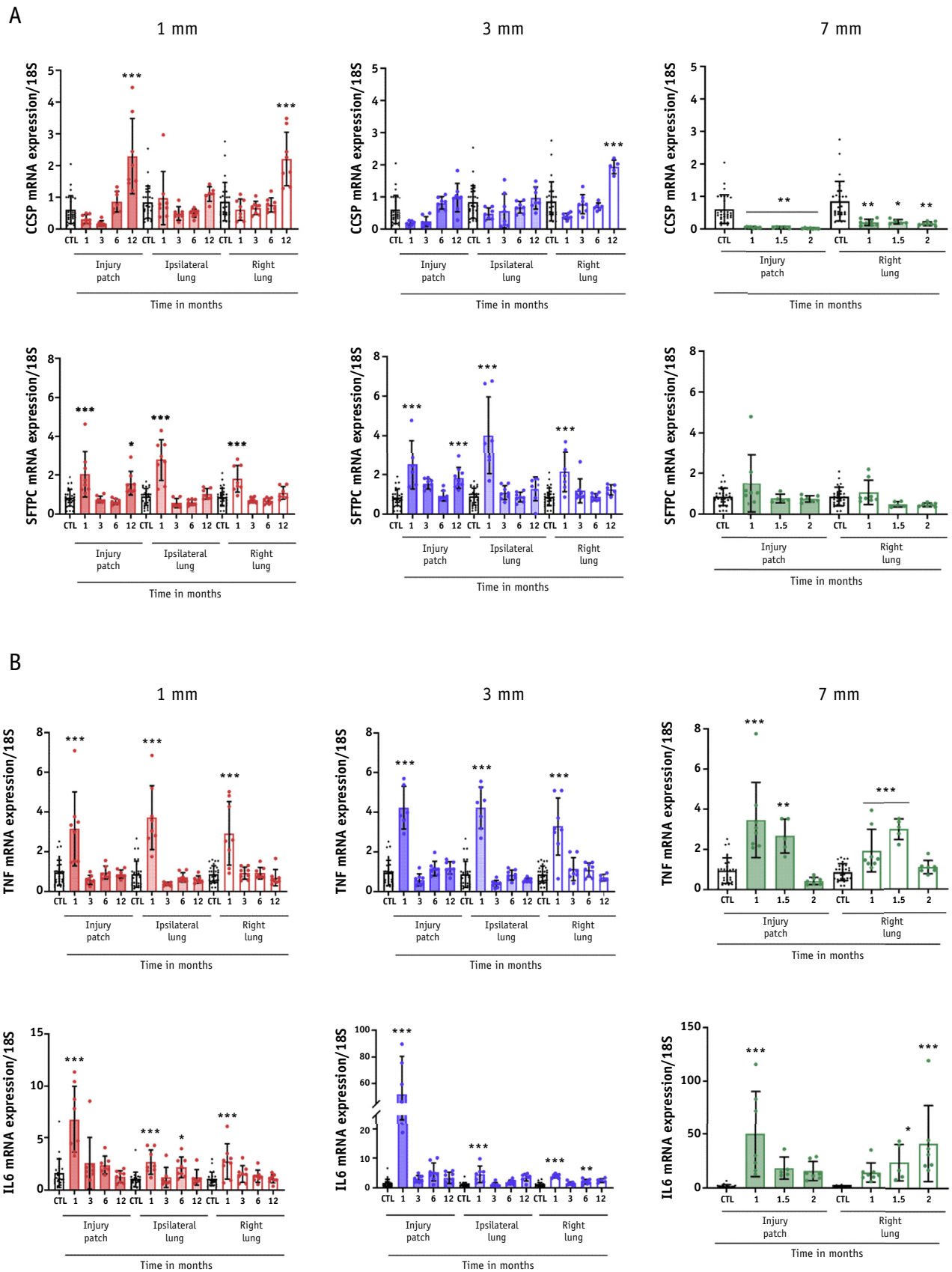
Fig. 4. Effect of varying beam size on mRNA expression. Changes in gene expression levels in the injury patch, ipsilateral lung, and right lung at different time points after 90 Gy exposure using 1-, 3-, or 7-mm collimation. (A) Examples of club cell (CCSP) and type II pneumocyte (SFTPC) markers. (B) Examples of inflammatory mediators TNF and IL6. $5 < n < 8$. Controls were pooled with $n = 29$. $*P < .05$. $**P < .01$. $***P < .001$.
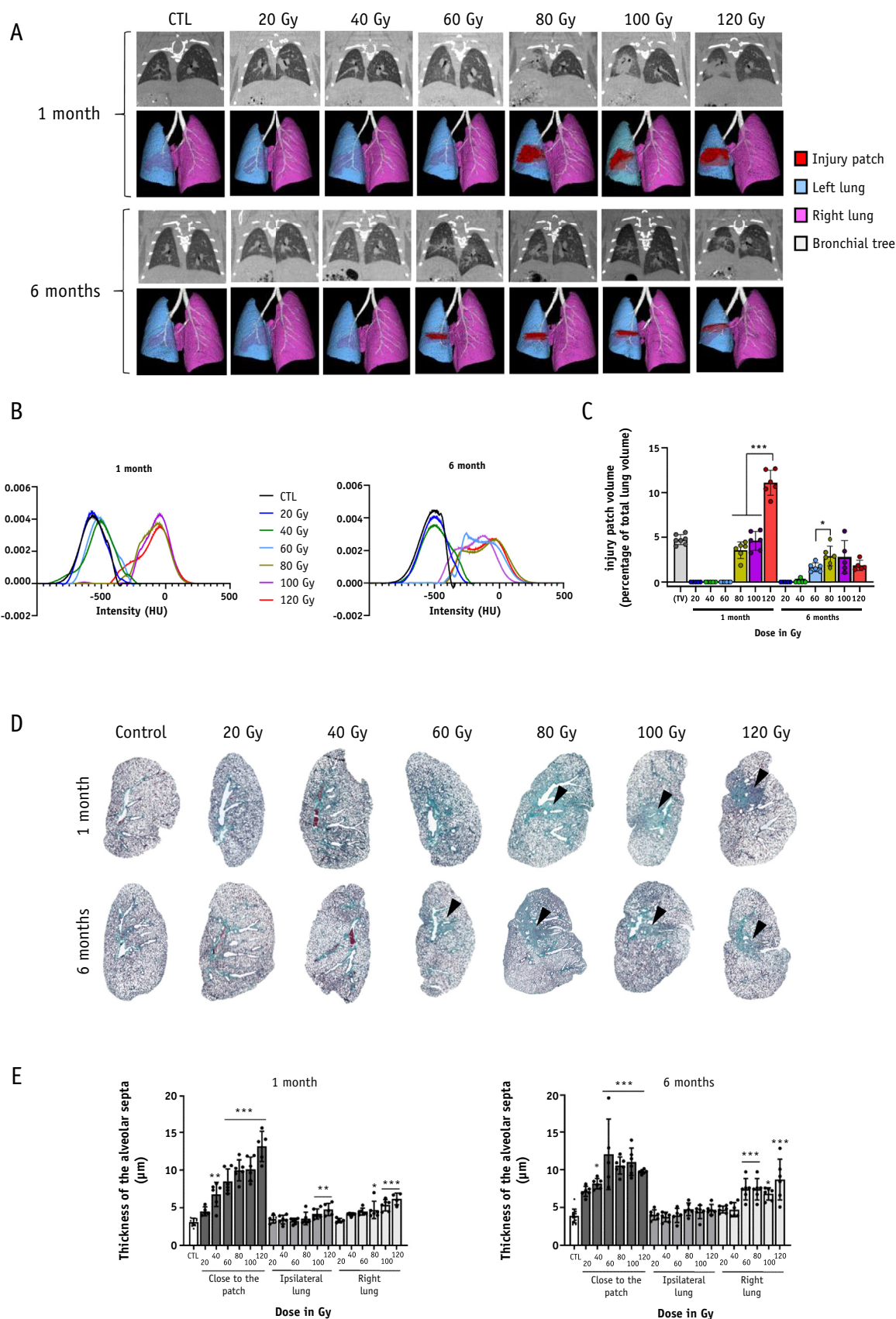
Fig. 5. Dose effect of left lung arc therapy. (A) Representative micro−computed tomography images and 3-dimensional reconstructions in controls and 1 and 6 months after exposure to 20, 40, 60, 80, 100, or 120 Gy. Different colors have been used to differentiate the injury patch (red), the left lung (blue), the right lung (pink), and the main bronchi (white). (B)

irradiation.[38] Here we show a strong increase in type II pneumocyte numbers in response to 90 Gy exposure with both 1-mm and 3-mm collimation. This was confirmed by SFTPC mRNA levels, suggesting attempts at tissue reconstruction. Further studies will be necessary to investigate whether this increase in type II pneumocyte numbers participates in tissue excessive scarring/fibrosis after focal ablative lung irradiation.

A limited irradiated volume using 3-mm beam collimation and arc irradiation in mice allowed dose escalation to 120 Gy without lethality. Three-millimeter beam collimation is a prerequisite to such dose escalation because 100 Gy irradiation using 5-mm collimation has been associated with a short survival time of 22 days.[11] We noted opacification at 1 month for doses of 80, 100, and 120 Gy, associated with severe alveolar septal thickening, major loss of club cells, and acute loss of type II pneumocytes. The increase in type II pneumocyte numbers was visible at 6 months for such high doses, suggesting delayed scarring. At 6 months, an injury patch appeared for the 60 Gy dose and was confirmed by a shift in the HU curve. Exposure to 20 Gy did not generate any club cell loss or alveolar septal thickening but increased type II pneumocyte number. Absence of sufficient club cell loss may explain the absence of tissue fibrosis at 6 months. Granton et al and Jin et al observed lung opacification after 20 Gy exposure using 5-mm and 7-mm beam collimation, respectively.[19,39] It is very difficult to compare published studies because of different dose deposition modalities. Discrepancies may, however, be explained by differences in irradiated volumes. Five- and 7-mm beam collimation without respiratory gating is probably close to hemithorax irradiation, a model in which 20 Gy can induce lung fibrosis.[40] Moreover, differences may come from observation times. In our case, fibrosis develops within 6 months, and one cannot rule out that 20-Gy, 3-mm focal irradiation may induce fibrosis within a longer period of time. This would merit further investigation.

Globally, when using 3-mm beam collimation, long-term (within 6 months) tissue fibrosis occurs for doses of 60 Gy or more. Very high doses generate acute opacification and rapid tissue fibrosis. The 60-Gy dose may be very interesting because it generates a severe acute tissue response with progression to fibrosis. This dose of 60 Gy is a high dose compared with the well-known 20-Gy dose

sufficient to induce fibrosis in models of wide-field lung exposure.[40] Using arc delivery and 3-mm beam collimation in mice, we previously showed that 5×20 Gy was necessary to obtain diffuse lung fibrosis within 15 months.[41] This single-dose range of 60 Gy is in accordance with reported data of focal lung exposure. Cho et al showed that using 3-mm collimator and dorsoventral delivery, mice exposed to 40 Gy developed insignificant fibrosis; those exposed to 100 Gy demonstrated lung fibrosis, suggesting, as said by the authors, a threshold dose between 40 and 100 Gy for lung fibrosis under these conditions.[11] The study by Hong et al[16] reported lung fibrosis from 40 Gy and maximum intensity after a single dorsoventral dose of 60 Gy or more using 2-mm beam collimation (6-week time point). Finally, Choi et al used the same dorsoventral dose delivery system with 3-mm beam collimation and observed a slight, followed by a marked, rise in collagen deposition at 2 and 6 months after 50 Gy exposure, respectively.[12] Lung fibrosis was rapid and severe after 90 Gy, but the study was stopped at 4 weeks, probably because of skin damage associated with dorsoventral delivery. Direct comparison between studies remains very challenging, however, because of differences in dose delivery modalities, generating varying irradiated lung volumes despite the use of the same beam collimation. For example, using 3-mm dorsoventral irradiation has been shown to represent 11.7%[16] and 12.6%[11] of the total lung volume in mice (volume in the beam path), whereas arc delivery in our case corresponds to 4.2% of the total lung volume. Data thus have to be considered not only according to beam collimation but also according to the dose delivery modalities (arc, single, or multibeams).

Another limitation to interpreting the effect of changes in beam collimation size is the absence of respiratory motion gating during dose delivery. This limitation is common to all published data on lung ablative focal irradiation given that, to our knowledge, no respiratory gating has been published until now for preclinical modeling of lung SBRT. Given an estimated range of less than 3 mm (Morgane Dos Santos, personal data), this may affect dose delivery for beam collimation less than 3 mm. This may be the case in our study using 1-mm beam collimation and may lead to decreased dose received by the tissue to the isocenter compared with the dose "prescribed" via the treatment planning system. This means that for 1-mm beam

---

Smoothed mean intensity representation in Hounsfield units (HU) in the injured area (patch when visible, left lung otherwise) at 1 (left panel) and 6 months (right panel) after radiation exposure to 20, 40, 60, 80, 100, or 120 Gy using 3-mm beam collimation compared with controls. $4 < n < 7$ per group. (C) Volume of the injury patch as a percentage of the total lung volume compared with a calculated theoretical target volume; n = 5 per point. For irradiated tissues, colors are the same as in (B). (D) Representative left lung histologic sections after Masson trichrome staining in control tissues and 1 month (upper line) and 6 months (lower line) after exposure to 20, 40, 60, 80, 100, or 120 Gy using 3-mm beam collimation. Arrowheads indicate visible injury patch. (E) Thickness of the alveolar septa measured in control tissues and close to the injury patch and the ipsilateral and right lungs 1 and 6 months after exposure to 20, 40, 60, 80, 100, and 120 Gy using 3-mm beam collimation; n = 6. $*P < .05$. $**P < .01$. $***P < .001$. (A color version of this figure is available at https://doi.org/10.1016/j.ijrobp.2020.03.011.)
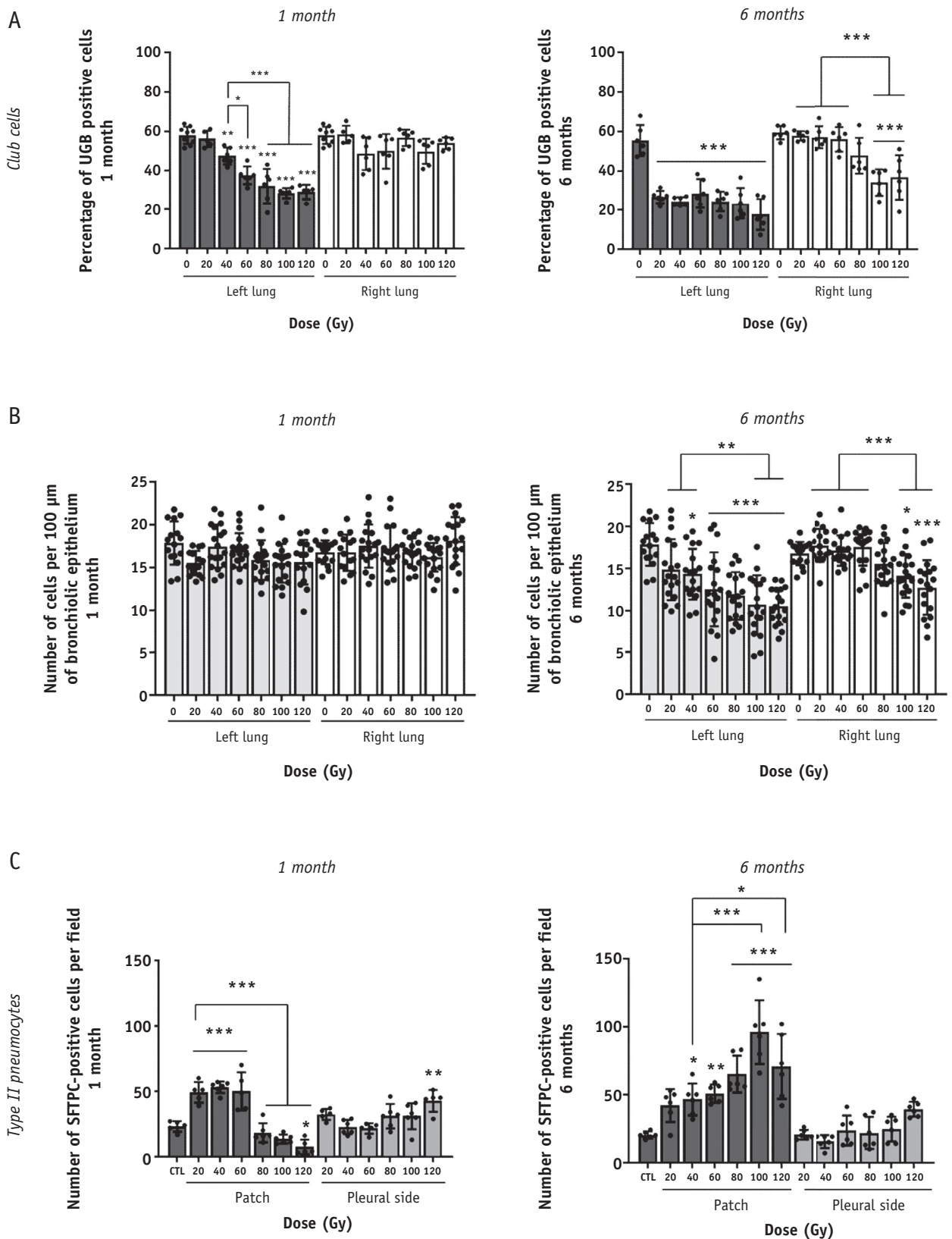
Fig. 6. Dose effect on club cells and type II pneumocyte numbers. (A) Percentages of UGB-positive cells in the bronchiolar epithelium of left and right lungs, 1 month (left panel) and 6 months (right panel) after exposure to 20, 40, 60, 80, 100, or 120 Gy using 3-mm beam collimation; n = 6. (B) Number of cells per 100 μm of bronchiolar epithelium measured in the left and right lungs 1 month (left panel) and 6 months (right panel) after exposure to 20, 40, 60, 80, 100, or 120 Gy using 3-mm beam collimation. 16 < n < 18. (C) Number of surfactant protein C-positive cells per field counted in the injury patch and pleural side 1 month (left panel) and 6 months (right panel) after exposure to 20, 40, 60, 80, 100, or 120 Gy using 3 mm beam collimation; n = 6. *P <.05. **P <.01. ***P <.001.

collimation, far more than 90 Gy prescribed to the isocenter may be necessary to induce lung fibrosis. This would have to be experimentally verified by a dose-escalation study, probably through very high prescribed doses to obtain tissue fibrosis with such collimation. The use of such high dose may become questionable in terms of clinical relevance.

Conclusions

Our study shows that arc delivery allows long-term studies of the response to high-dose radiation exposure of the mouse left lung when limiting field size. Focal lung fibrosis development is associated with both club cell loss and increased type II pneumocyte numbers. In our conditions, using 3-mm beam collimation and a single dose of 60 Gy allows development of lung fibrosis over a time span compatible with the life span of mice. Further studies will be necessary to implement this model, particularly concerning very small volumes necessitating respiratory motion gating to ensure matching of the prescribed dose to the planning system and the dose received by the target volume. The development of accurate preclinical models will allow pertinent future studies to improve understanding of SBRT radiobiology and develop therapeutic strategies whose mitigating power will depend on the presence of both high-dose irradiated areas and spared structures.

References

1. Macià i Garau M. Radiobiology of stereotactic body radiation therapy. *Rep Pract Oncol Radiother* 2017;22:86-95.
2. Thompson M, Rosenzweig KE. The evolving toxicity profile of SBRT for lung cancer. *Transl Lung Cancer Res* 2019;8:48-57.
3. Cosset JM, Mornex F, Eschwege F. [Hypofractionation and radiotherapy: "The eternal return"]. *Cancer Radiother* 2013;17:355-362.
4. Timmerman R, McGarry R, Yiannoutsos C, et al. Excessive toxicity when treating central tumors in a phase II study of stereotactic body radiation therapy for medically inoperable early-stage lung cancer. *J Clin Oncol* 2006;24:4833-4839.
5. Roach M 3rd, Gandara DR, Yuo HS, et al. Radiation pneumonitis following combined modality therapy for lung cancer: Analysis of prognostic factors. *J Clin Oncol* 1995;13:2606-2612.
6. Johansson S, Svensson H, Denekamp J. Timescale of evolution of late radiation injury after postoperative radiotherapy of breast cancer patients. *Int J Radiat Oncol Biol Phys* 2000;48:745-750.
7. Thames HD Jr, Withers HR, Peters LJ, et al. Changes in early and late radiation responses with altered dose fractionation: Implications for dose-survival relationships. *Int J Radiat Oncol Biol Phys* 1982;8:219-226.
8. Guckenberger M, Baier K, Polat B, et al. Dose-response relationship for radiation-induced pneumonitis after pulmonary stereotactic body radiotherapy. *Radiother Oncol* 2010;97:65-70.
9. Matsuo Y, Shibuya K, Nakamura M, et al. Dose–volume metrics associated with radiation pneumonitis after stereotactic body radiation therapy for lung cancer. *Int J Radiat Oncol Biol Phys* 2012;83:e545-e549.
10. Lo SS, Sahgal A, Chang EL, et al. Serious complications associated with stereotactic ablative radiotherapy and strategies to mitigate the risk. *Clin Oncol (R Coll Radiol)* 2013;25:378-387.
11. Cho J, Kodym R, Seliounine S, et al. High dose-per-fraction irradiation of limited lung volumes using an image-guided, highly focused irradiator: Simulating stereotactic body radiotherapy regimens in a small-animal model. *Int J Radiat Oncol Biol Phys* 2010;77:895-902.
12. Choi SH, Hong ZY, Nam JK, et al. A hypoxia-induced vascular endothelial-to-mesenchymal transition in development of radiation-induced pulmonary fibrosis. *Clin Cancer Res* 2015;21:3716-3726.
13. Kwon OS, Kim KT, Lee E, et al. Induction of MiR-21 by stereotactic body radiotherapy contributes to the pulmonary fibrotic response. *PloS One* 2016;11:e0154942.
14. Hong ZY, Eun SH, Park K, et al. Development of a small animal model to simulate clinical stereotactic body radiotherapy-induced central and peripheral lung injuries. *J Radiat Res* 2014;55:648-657.
15. Hong ZY, Song KH, Yoon JH, et al. An experimental model-based exploration of cytokines in ablative radiation-induced lung injury in vivo and in vitro. *Lung* 2015;193:409-419.
16. Hong ZY, Lee CG, Shim HS, et al. Time, dose, and volume responses in a mouse pulmonary injury model following ablative irradiation. *Lung* 2016;194:81-90.
17. Sharplin J, Franko AJ. A quantitative histological study of strain-dependent differences in the effects of irradiation on mouse lung during the early phase. *Radiat Res* 1989;119:1-14.
18. Sharplin J, Franko AJ. A quantitative histological study of strain-dependent differences in the effects of irradiation on mouse lung during the intermediate and late phases. *Radiat Res* 1989;119:15-31.
19. Jin H, Jeon S, Kang GY, et al. Identification of radiation response genes and proteins from mouse pulmonary tissues after high-dose per fraction irradiation of limited lung volumes. *Int J Radiat Biol* 2017;93:184-193.
20. Lavigne J, Suissa A, Verger N, et al. Lung stereotactic arc therapy in mice: development of radiation pneumopathy and influence of HIF-1alpha endothelial deletion. *Int J Rad Oncol Biol Phys* 2019;104:279-290.
21. Frakulli R, Salvi F, Balestrini D, et al. Radiological differential diagnosis between fibrosis and recurrence after stereotactic body radiation therapy (SBRT) in early stage non-small cell lung cancer (NSCLC). *Transl Lung Cancer Res* 2017;6:S1-S7.
22. van Berlo D, Khmelinskii A, Gasparini A, et al. Micro cone beam computed tomography for sensitive assessment of radiation-induced late lung toxicity in preclinical models. *Radiother Oncol* 2019;138:17-24.
23. De Ruysscher D, Granton PV, Lieuwes NG, et al. Nintedanib reduces radiation-induced microscopic lung fibrosis but this cannot be monitored by CT imaging: A preclinical study with a high precision image-guided irradiator. *Radiother Oncol* 2017;124:482-487.
24. Nadkarni RR, Abed S, Draper JS. Stem cells in pulmonary disease and regeneration. *Chest* 2018;153:994-1003.
25. Perl AK, Riethmacher D, Whitsett JA. Conditional depletion of airway progenitor cells induces peribronchiolar fibrosis. *Am J Respir Crit Care Med* 2011;183:511-521.
26. Aoshiba K, Tsuji T, Itoh M, et al. A murine model of airway fibrosis induced by repeated naphthalene exposure. *Exp Toxicol Pathol* 2014;66:169-177.
27. Yokoyama T, Yanagihara T, Suzuki K, et al. Depletion of club cells attenuates bleomycin-induced lung injury and fibrosis in mice. *J Inflamm (Lond)* 2017;14:20.
28. Manning CM, Johnston CJ, Hernady E, et al. Exacerbation of lung radiation injury by viral infection: The role of clara cells and clara cell secretory protein. *Radiat Res* 2013;179:617-629.
29. Barkauskas CE, Cronce MJ, Rackley CR, et al. Type 2 alveolar cells are stem cells in adult lung. *J Clin Invest* 2013;123:3025-3036.
30. Jansing NL, McClendon J, Henson PM, et al. Unbiased quantitation of alveolar type II to alveolar type I cell transdifferentiation during repair after lung injury in mice. *Am J Respir Cell Mol Biol* 2017;57:519-526.
31. Skronska-Wasek W, Mutze K, Baarsma HA, et al. Reduced frizzled receptor 4 expression prevents wnt/beta-catenin-driven alveolar lung repair in chronic obstructive pulmonary disease. *Am J Respir Crit Care Med* 2017;196:172-185.

32. Kasper M, Haroske G. Alterations in the alveolar epithelium after injury leading to pulmonary fibrosis. *Histol Histopathol* 1996;11:463-483.

33. Sisson TH, Mendez M, Choi K, et al. Targeted injury of type II alveolar epithelial cells induces pulmonary fibrosis. *Am J Respir Crit Care Med* 2010;181:254-263.

34. Osterreicher J, Pejchal J, Skopek J, et al. Role of type II pneumocytes in pathogenesis of radiation pneumonitis: Dose response of radiation-induced lung changes in the transient high vascular permeability period. *Exp Toxicol Pathol* 2004;56:181-187.

35. Citrin DE, Shankavaram U, Horton JA, et al. Role of type II pneumocyte senescence in radiation-induced lung fibrosis. *J Natl Cancer Inst* 2013;105:1474-1484.

36. Coggle JE. Proliferation of type II pneumonocytes after x-irradiation. *Int J Radiat Biol Relat Stud Phys Chem Med* 1987;51:393-399.

37. Lavigne J, Soysouvanh F, Buard V, et al. Conditional plasminogen activator inhibitor type 1 deletion in the endothelial compartment has no beneficial effect on radiation-induced whole lung damage in mice. *Int J Radiat Oncol Biol Phys* 2017;99:972-982.

38. Almeida C, Nagarajan D, Tian J, et al. The role of alveolar epithelium in radiation-induced lung injury. *PloS One* 2013;8:e53628.

39. Granton PV, Dubois L, van Elmpt W, et al. A longitudinal evaluation of partial lung irradiation in mice by using a dedicated image-guided small animal irradiator. *Int J Radiat Oncol Biol Phys* 2014;90:696-704.

40. Beach TA, Groves AM, Williams JP, et al. Modeling radiation-induced lung injury: Lessons learned from whole thorax irradiation. *Int J Radiat Biol* 2020;96:129-144.

41. Soysouvanh F, Benadjaoud MA, Dos Santos M, et al. Stereotactic lung irradiation in mice promotes long-term senescence and lung injury. *Int J Radiat Oncol Biol Phys* 2020;106:1017-1027.